March 2024. Horticultural Plant Journal, 10 (2): 355–366

Horticultural Plant Journal

Available online at www.sciencedirect.com
The journal's homepage: http://www.keaipublishing.com/en/journals/horticultural-plant-journal

Insights into the dwarfing mechanism of pear (*Pyrus betulaefolia*) based on anatomical and structural analysis using X-ray scanning

Lili Dong [a,1], *Chuxuan Yang* [a,1], *Jing Wang* [a], *Jingjing Li* [a], *Mei Zhao* [b], *Dingli Li* [a], *Zhiyun Qiu* [a], *Chunhui Ma* [a,*], *and Zhenhua Cui* [a,*]

[a] *College of Horticulture, Qingdao Agricultural University, Qingdao, Shandong 266109, China*
[b] *College of Landscape and Forestry, Qingdao Agricultural University, Qingdao, Shandong 266109, China*

Received 15 December 2022; Received in revised form 22 February 2023; Accepted 15 March 2023

Available online 7 June 2023

A B S T R A C T

The lack of a suitable rootstock to control scion growth has limited the development of high-density plantations in pear production, which is partly attributed to poor understanding of the dwarfing mechanism. In the present study, the rootstock of the dwarf-type pear (*Pyrus betulaefolia*) 'PY-9' was identified and used as the material for anatomical analysis. 'PY-9' grew to half the tree height of the normal cultivar 'Zhengdu', along with fewer internodes and shorter length. Significant differences in growth rate between 'PY-9' and 'Zhengdu' were detected at approximately 30 days after full bloom, which corresponded with the time of the greatest difference in water potential between the dwarf and normal cultivar. 'PY-9' showed a higher photosynthetic rate than 'Zhengdu'. Anatomical analysis showed that 'PY-9' had higher area ratios of both phloem and xylem and more developed vascular tissues than 'Zhengdu'. The three-dimensional reconstructed skeleton of the xylem from X-ray computed tomography scanning revealed greater intervessel connectivity in 'Zhengdu' than in 'PY-9', which could contribute to the more vigorous growth of 'Zhengdu'. This study thus provides the first comparison of the microstructural properties of xylem elements between a dwarfing-type and vigorous-type pear rootstock, providing new insights into the dwarfing mechanism in pear and facilitating breeding of dwarf pear rootstocks to increase crop productivity.

Keywords: *Pyrus betulaefolia*; Anatomical analysis; Dwarfing mechanism; Intervessel connectivity; Rootstock

1. Introduction

Pear (*Pyrus* spp.) is one of the most commercially important fruit trees, which has a long history of cultivation worldwide (Wu et al., 2013). To obtain higher profits, the use of dwarfing cultivars and high-density plantations has become common in modern fruit production systems, which save manual labor, facilitate mechanical operations, and induce precocity (Cui et al., 2021). Grafting is an important means to minimize the size of a fruit tree, in addition to conferring favorable characteristics on the scion and improving the fruit quality (Venema et al., 2008; Petri et al., 2018; Yan et al., 2022; Marín et al., 2023). However, the lack of suitable rootstocks to effectively control the growth of the grafted scions has limited the development of dwarfed pear orchards (Weibel, 2008). Compared to apple, fewer studies and efforts have been made to understand the mechanism by which rootstocks result in a dwarfed tree phenotype in pear, making it difficult to develop ideal dwarfing rootstocks in pear (Knäbel

[1] These authors contributed equally to this work.
* Corresponding authors.
E-mail addresses: machunhui2000@163.com; zhcui@qau.edu.cn
Peer review under responsibility of Chinese Society of Horticultural Science (CSHS) and Institute of Vegetables and Flowers (IVF), Chinese Academy of Agricultural Sciences (CAAS)

https://doi.org/10.1016/j.hpj.2023.03.013
2468-0141/Copyright © 2023 Chinese Society for Horticultural Science (CSHS) and Institute of Vegetables and Flowers (IVF), Chinese Academy of Agricultural Sciences (CAAS). Publishing services by Elsevier B.V. on behalf of KeAi Communications Co. Ltd. This is an open access article under the CC BY-NC-ND license (http://creativecommons.org/licenses/by-nc-nd/4.0/).

et al., 2015). Therefore, clarification of the mechanisms involved in the reduction of the scion size due to the properties of the rootstock is important to accelerate the breeding of pear rootstocks to meet current demand.

Various theories have been proposed to explain the mechanisms by which the rootstock reduces the growth of a fruit tree. In apple, three quantitative trait loci (QTLs) associated with rootstock-induced dwarfing were identified as *Dw1*, *Dw2*, and *Dw3*, which are located on chromosome 5, 11, and 13, respectively (Pilcher et al., 2008; Fazio et al., 2014; Foster et al., 2015; Harrison et al., 2016). In pear, a QTL (*PcDw1*) associated with flowering traits and tree vigor was identified in linkage group 5 (LG5) on chromosome 5, which was determined to be syntenic to the apple 'M9' rootstock *Dw1* locus at the upper end of LG5 (Knäbel et al., 2015). An attempt to identify the dwarfing-associated genes using Chinese dwarf pear 'Zhongai 1' and non-dwarf pear 'Jinxiang' through transcriptome analysis found many genes are likely involved in the dwarfing mechanism, suggesting the complexity of the dwarfing mechanism in pear trees (Li et al., 2015; Ou et al., 2015).

In addition to studies performed at the genetic level, alterations of hormone concentrations, compounds metabolism, and vascular structures have also been proposed to play roles in rootstock-induced dwarfing and have thus attracted research attention (Weibel, 2008). Yan et al. (2022) recently reported that zeatin-riboside and abscisic acid levels correlated with dwarfing phenotypes of four apple germplasms, which was supported by the expression levels of the genes associated with the synthesis of these hormones. A recent study suggested that over-accumulation of abscisic acid resulted in a dwarf phenotype of pear tree (Liu et al., 2022). Cui et al. (2021) found that flavonoids and phenolic acids/derivatives were the key compounds contributing to the interstock-induced dwarfing pear tree phenotype. Previous studies also suggested that the root bark percentage of the apple rootstock was associated with tree vigor (Harrison et al., 2016). In peach, the xylem vessel characteristic of the rootstock has been shown to directly influence tree growth (Tombesi et al., 2010), and the dwarfing rootstock of cherry was considered to alter the vessel characteristics of the scion and the healing of graft union, resulting in reduced tree growth (Olmstead, 2006). These data indicate that differences in the vascular anatomical characteristics of rootstocks appear to influence the growth of the scions. Despite extensive efforts to uncover how the rootstock alters the growth of trees from several aspects, the specific mechanism underlying rootstock-induced dwarfing remains to be fully elucidated.

Pyrus betulaefolia is a widely used and favored pear rootstock in northern China owing to its good compatibility with many pear cultivars, and strong tolerance to cold, salinity, drought, and other environmental stresses. However, *P. betulaefolia* is a very vigorous species, and the excessive growth of the grafted scions has limited its application in establishing dwarfed pear orchards. We previously reported a new dwarfing phenotype of *P. betulaefolia* identified in Puyu county, China, which was named 'PY-9', exhibiting characteristics of a smaller size and more compact tree body than the normal *P. betulaefolia* 'Zhengdu'. 'PY-9' showed a stable dwarfing morphology after being transferred to our germplasm nursery in 2010, indicating its potential as a rootstock for dwarfing planting in pear orchards.

To confirm this possibility, the aim of the present study was to compare the morphological, physiological, and anatomical characteristics of the rootstocks between the dwarfing 'PY-9' and normal 'Zhengdu'. These results can thus provide useful information for rootstock selection in production along with offering further insights into the dwarfing mechanisms of fruit trees.

2. Materials and methods

2.1. Materials

The dwarfing *P. betulaefolia* 'PY-9' rootstock was transplanted to Jiaozhou Experimental Station of Qingdao Agricultural University (120.09°E, 36.44°N) from its original location by grafting onto 1-year-old callery pear (*Pyrus calleryana*) seedlings in June, 2010. The normal *P. betulaefolia* 'Zhengdu' rootstock is conserved at the same nursery under the same conditions as 'PY-9'. *In vitro* tissue cultures of the two genotypes were established using the tips of the 1-year-old shoot collected in the growing season after surface sterilization in May, 2018. The 10-year-old 'PY-9'/*P. calleryana* and 'Zhengdu'/*P. calleryana* field-grown plants and *in vitro*-grown plantlets were used for measurements in the present analysis.

2.2. Morphological analysis

The tree height, leaf morphological indices, and fruit characteristics of the field-grown 'PY-9' and 'Zhengdu' pear trees were measured in October from 2018 to 2020. The width and length of leaf, and the length and diameter of shoot, and fruit diameters were measured using a digital caliper. The thickness of the leaf was measured using a thickness gauge (SM114, Teclock, Japan). The leaf area was measured using a leaf area meter (Yaxin-1241, Beijing, China). The fresh weight of the fruit was determined using a digital scale. Images were captured by a digital camera (Canon, Japan). Ten samples were measured from each tree, and 5 trees were used as biological repeats for each cultivar.

In vitro-grown 'PY-9' and 'Zhengdu' plantlets were cultured on a basal medium (4.4 $g \cdot L^{-1}$ MS + 30 $g \cdot L^{-1}$ sucrose + 7 $g \cdot L^{-1}$ agar, pH 5.8) supplemented with 1.0 $mg \cdot L^{-1}$ 6-benzylaminopurine and 0.3 $mg \cdot L^{-1}$ indole-3-butyric acid. The *in vitro* plantlets were maintained at a constant temperature of (24 ± 2) °C under a 16-h photoperiod with a light intensity of 3000 lx provided by white fluorescent tubes.

2.3. Growth and physiological analysis

The growth parameters including plant height, number of branches, fresh weight and dry weight of the *in vitro* plantlets were investigated at 8 weeks of growth. Thirty samples were used for the measurement of the growth parameters every time, and the whole experiments were repeated 3 times.

For the field-grown trees, the length of the 1-year-old shoot was recorded every 10 days from April to June before growth cessation. The water potential of the 1-year-old shoot (Ψ_{stem}) was determined using a pressure chamber (Scholander et al., 1965) according to the methods described by Knipfer et al. (2015a). Ψ_{stem} was measured on eight leaves covered with a sealed and foiled plastic bag for more than 20 min. The leaves were excised at the base of the petioles and immediately placed into the

chamber with the petiole end protruding out of the chamber. Slow pressure was applied on the chamber (0.03 MPa·s^{-1}) until water emerged from the excised petiole surface and the corresponding pressure was recorded as Ψ_{stem}. The measurement was carried out at 14:00–15:00 when transpiration was at its daily maximum.

The chlorophyll content of the mature leaves of the field-grown trees was determined according to the method described by Li et al. (2013). Briefly, chlorophyll of the fresh leaves collected in June was extracted using 80% acetone incubated at (22 ± 2) °C in the dark over night. Absorbance of the extract was read at 663 nm and 645 nm with a spectrophotometer (Thermo Miltiskan MK3, USA). Then chlorophyll a (Chl a), chlorophyll b (Chl b) and total Chlorophyll (Chl T) were calculated as: Chl a (mg·g^{-1} FW) = [12.7 (D_{663})–2.69 (D_{645})] × FV/1000 × TFW; Chl b (mg·g^{-1} FW) = [22.9(D_{645})–4.68 (D_{663})] × FV/1000 × TFW; and Chl T (mg·g^{-1} FW) = [20.2 (D_{645})–8.02 (D_{6663})] × V/1000 × TFW, in which FW represents fresh weight, D represents the optical density with a corresponding reading wavelength (nm), FV represents the final volume (mL) of chlorophyll extract, TFW represents the total fresh weight (g) of leaves used for extraction. The photosynthetic activity was investigated in June using a CIRAS-3 Portable Photosynthesis System (PP Systems, USA), according to the methods described by Liu et al. (2022). Briefly, the net photosynthetic rate (P_n), intercellular CO_2 concentration (C_i), transpiration rate (T_r), and stomatal conductance (G_s) were measured with the following settings: relative humidity, 40% ± 3%; carbon dioxide concentration, 390 μmol·mol^{-1}; light-emitting diode light source, 1200 μmol·m^{-2}·s^{-1}; red light, 90%; and blue light, 10%. The data were recorded only after the measurements became stable. Three mature leaves of the 1-year-old shoots from different directions were selected for the measurements, and the experiment was carried out at 10:00–11:00 in the morning.

For the field measurement of growth rate, water potential, chlorophyll content and the photosynthetic parameters, 5 trees of each cultivar were used as biological repeats, and the whole experiments were repeated three times from 2018 to 2020.

2.4. Anatomical analysis

The roots, stems, petioles, and leaves were excised from 8-week-old *in vitro*-grown plantlets for histological observations according to Cui et al. (2019). Briefly, samples were fixed with a solution consisting of 50% ethanol/formalin/acetic acid (18:1:1) for 24 h, followed by dehydration in a series of solutions of ethanol increasing from 50%, 70%, 85%, 95%, to 100% for 3 h per solution. After being embedded in paraffin, sections (5 μm in thickness) were obtained using a rotary microtome (Leica RM 2235, Leica, Wetzlar, Germany). Sections were stained using 0.1% toluidine blue and observed with the aid of light microscopy (Leica DM 2235). Ten samples of both 'PY-9' and 'Zhengdu' were used for the anatomical observation.

2.5. X-ray computed tomography scanning

For the field-grown trees, the structural properties of the mature shoots were analyzed using X-ray computed tomography scanning (nanoVoxel-3502E system, Sanying Precision Instruments Co., Ltd., Tianjin) according to Cui et al. (2022). Briefly, the middle part of 1-year-old shoot of 2 cm in length (collected in December, 2020) was rotated on the stage at an increment of 0.2° over a total of 360° at 25 °C, yielding a total of 1800 two-dimensional (2D) projection images. Transverse and longitudinal section slices were generated from the shadow projections using the Feldkamp reconstruction algorithm (Feldkamp et al., 1984). The 2D projection images were visualized using OCTOPUS 8.6 software (Institute for Nuclear Sciences, Ghent University, Ghent, Belgium), and the three-dimensional (3D) images were reconstructed using Avizo 8.1 software (Thermo Fisher Scientific, China). A threshold of 5840 grayscale was used as a discriminative value for the separation of pores and tissues. The size of the pores and the porosity of the tissues from the pith to the phloem were evaluated using the data of a 100 μm × 100 μm area after segmentation. The scanning data of a 100 μm × 100 μm × 300 μm volume of the pith, xylem, and phloem tissues, respectively, were extracted to analyze the surface area, which was calculated as the number of pixels on the surface, including both the exterior and interior surface. The settings used for X-ray scanning are listed in Table 1. To obtain more details of the structural and spatial arrangement of the vessels, the connectivity and the skeleton information were analyzed using the 3D networks with the aid of Avizo 8.1 software. Three biological repeats were used for both 'PY-9' and 'Zhengdu' in the X-ray scanning analysis.

2.6. Statistical analysis

Analysis of variance or Student's *t*-test was performed for comparisons between groups using DPS 7.05 software (Zhejiang University).

3. Results

3.1. Morphological comparison between 'PY-9' and 'Zhengdu' pear

After grafted growth for 10 years, 'Zhengdu' showed a larger tree body, with a tree height above 5 m and a tree crown diameter of 3.8 m, compared with 'PY-9', with a less than 3 m tree height and 2.4 m tree crown diameter (Fig. 1, A and B; Table 2). The shoot length of 'Zhengdu' was also much longer than that of 'PY-9' (Fig. 1, C). Correspondingly, the internode length and internode

Table 1 Settings of X-ray scanning used in this study

Sample	Source origin distance/source origin detector distance/mm	Pixel size/μm	Voltage/kV	Current/μA	Scanning time/h
'PY-9'	6.84/172.05	2	60	70	0.2
'Zhengdu'	6.24/126.78	2	60	70	0.2



Fig. 1 Morphological comparison of 'PY-9' and 'Zhengdu'

A - B. Ten-year-old 'PY-9' (A) and 'Zhengdu' (B) trees. The length of the cement pillars in both photographs is 3 m. C. One-year-old shoots of 'PY-9' (left) and 'Zhengdu' (right). (D) Leaves of 'PY-9' (left) and 'Zhengdu' (right). (E) Fruits of 'PY-9' (left) and 'Zhengdu' (right). (F) *In vitro* plantlets of 'PY-9' (left) and 'Zhengdu' (right).

Table 2 Morphological comparison of 'PY-9' and 'Zhengdu'

Sample	Tree body and 1-year-old shoot				
	Tree height/m	Crown diameter/m	Shoot diameter/mm	Internode No.	Internode length/cm
'PY-9'	< 3	2.4 ± 0.3 b	5.9 ± 1.0 a	10 ± 1.2 b	1.5 ± 0.2 b
'Zhengdu'	> 5	3.8 ± 0.5a	3.9 ± 0.8 b	15 ± 2.1 a	3.5 ± 0.5 a
Sample	Leaf				
	Petiole length/cm	Leaf width/cm	Leaf length/cm	Leaf area/cm^2	Leaf thickness/mm
'PY-9'	4.0 ± 0.2 a	3.4 ± 0.1 a	5.7 ± 0.2 a	14.4 ± 0.5 a	0.20 ± 0.04 a
'Zhengdu'	3.8 ± 0.2 a	2.6 ± 0.1 b	5.3 ± 0.2 a	9.3 ± 0.4 b	0.17 ± 0.02 b
Sample	Fruit				
	Peduncle length/cm	Peduncle diameter/mm	Vertical diameter/mm	Transverse diameter/mm	Weight/g
'PY-9'	1.8 ± 0.3 a	2.1 ± 0.3 a	10.0 ± 1.0 a	11.2 ± 1.0 a	5.9 ± 0.9 a
'Zhengdu'	2.2 ± 0.3 a	1.9 ± 0.2 a	9.1 ± 1.2 a	9.3 ± 0.7 b	4.6 ± 0.3 b

Note: Data are presented as means ± *SD* of three replicate experiments. Different letters following the values for the same parameters indicate significant differences at $P < 0.05$.

number of the 'Zhengdu' shoot were also greater than those of the 'PY-9' shoot (Table 2). However, the 'PY-9' shoot had a greater diameter than that of the 'Zhengdu' shoot (Fig. 1, C; Table 2). Compared with those of 'Zhengdu', 'PY-9' showed a greater leaf width, leaf thickness, and leaf area. No difference in the petiole length or leaf length between 'PY-9' and 'Zhengdu' was observed (Fig. 1, D; Table 2). The fruits of both 'Zhengdu' and 'PY-9' showed the same clay-bank color. However, 'PY-9' fruits had a greater transverse diameter and weight than those of 'Zhengdu' (Fig. 1, E; Table 2).

Table 3 Growth parameters of eight-week-old *in vitro*-grown plantlets of 'PY-9' and 'Zhengdu'

Sample	Plant height/cm	Number of branches	Fresh weight/g	Dry weight/mg
'PY-9'	5.5 ± 0.5 a	3 ± 0.8 b	0.81 ± 0.04 b	50.2 ± 7.5 a
'Zhengdu'	6.5 ± 0.7 a	6 ± 1.2 a	0.95 ± 0.08 a	57.3 ± 8.0 a

Note: Data are means ± *SD* of three replicate experiments. Different letters following the values for the same parameters indicate significant differences at $P < 0.05$.

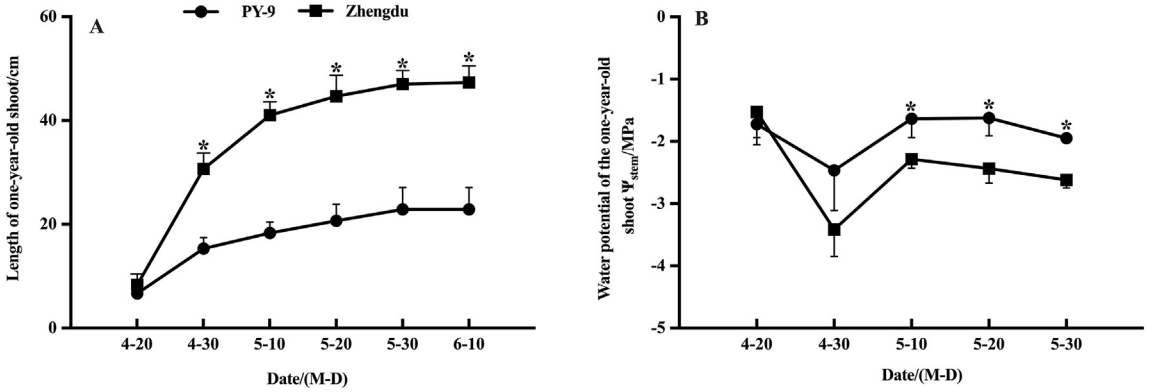


Fig. 2 Comparison of shoot growth and its water potential of 'PY-9' and 'Zhengdu'

(A) Shoot length of 'PY-9' and 'Zhengdu' during the growing season. (B) Changes of water potential during the growing season. Date points represent mean ± *SD* of three replicate experiments. * means significant differences at the corresponding time point at $P < 0.05$.

3.2. *Growth and physiology comparison*

When cultured on medium *in vitro*, 'Zhengdu' produced more branches than 'PY-9', resulting in a greater fresh weight of 'Zhengdu' (Fig. 1, F; Table 3). There was no significant difference in the plant height or dry weight between 'Zhengdu' and 'PY-9' (Table 3). When grown in the field, the 1-year-old shoot of 'Zhengdu' (48 cm) was much longer than that of 'PY-9' (25 cm) at growth cessation in late June (Fig. 2, A). A higher growth rate of the 'Zhengdu' shoot was observed from April 20th (20 days after full bloom) to May 10th (40 days after full bloom) than that of 'PY-9' for the same period (Fig. 2, A). During the growing season, 'Zhengdu' exhibited a greater water potential tension than that of 'PY-9' (Fig. 2, B). Both 'Zhengdu' and 'PY-9' showed the greatest water potential tension on April 30th (30 days after full bloom) (Fig. 2, B), indicating a fast-growing time point. With respect to the photosynthetic characteristics, 'PY-9' showed a much higher level of Chl a content in the leaves than 'Zhengdu',

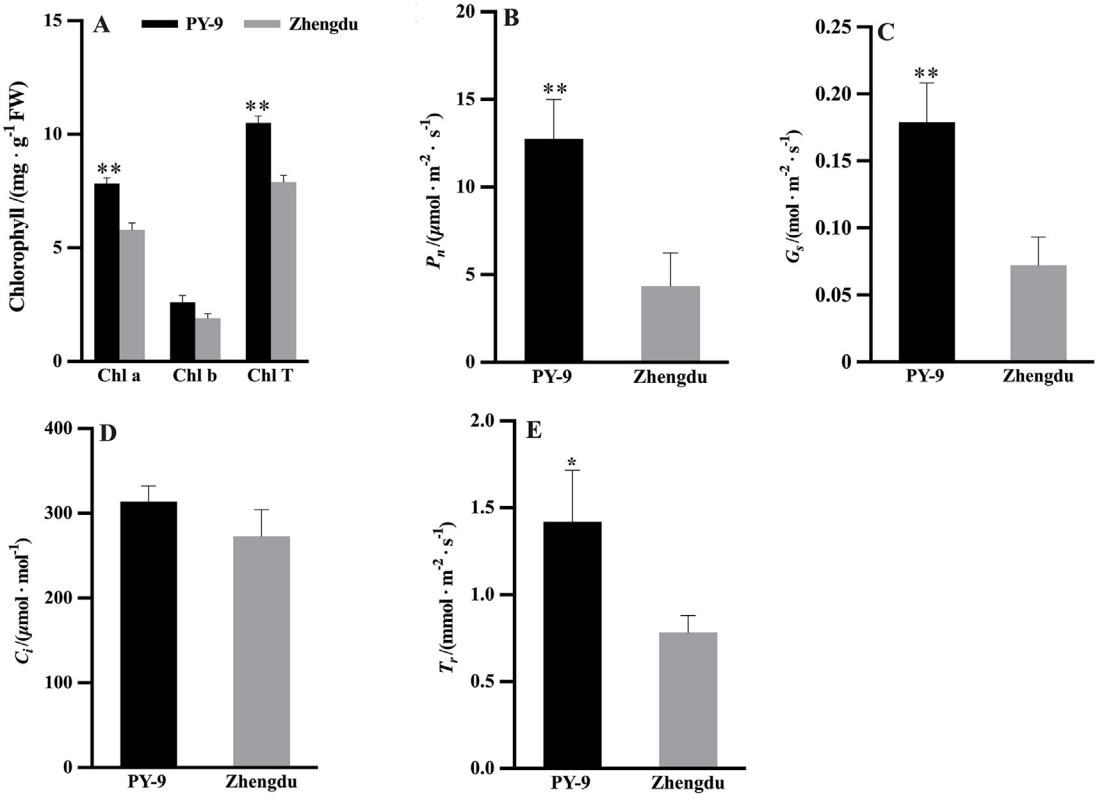


Fig. 3 Comparison of photosynthetic parameters of 'PY-9' and 'Zhengdu'

(A) chlorophyll content, (B) net photosynthetic rate (P_n), (C) stomatal conductance (G_s), (D) intercellular CO_2 concentration (C_i), (E) transpiration rate (T_r). Bars represent mean ± *SD* of three replicate experiments. * and ** mean significant differences at $P < 0.05$ and $P < 0.01$, respectively.

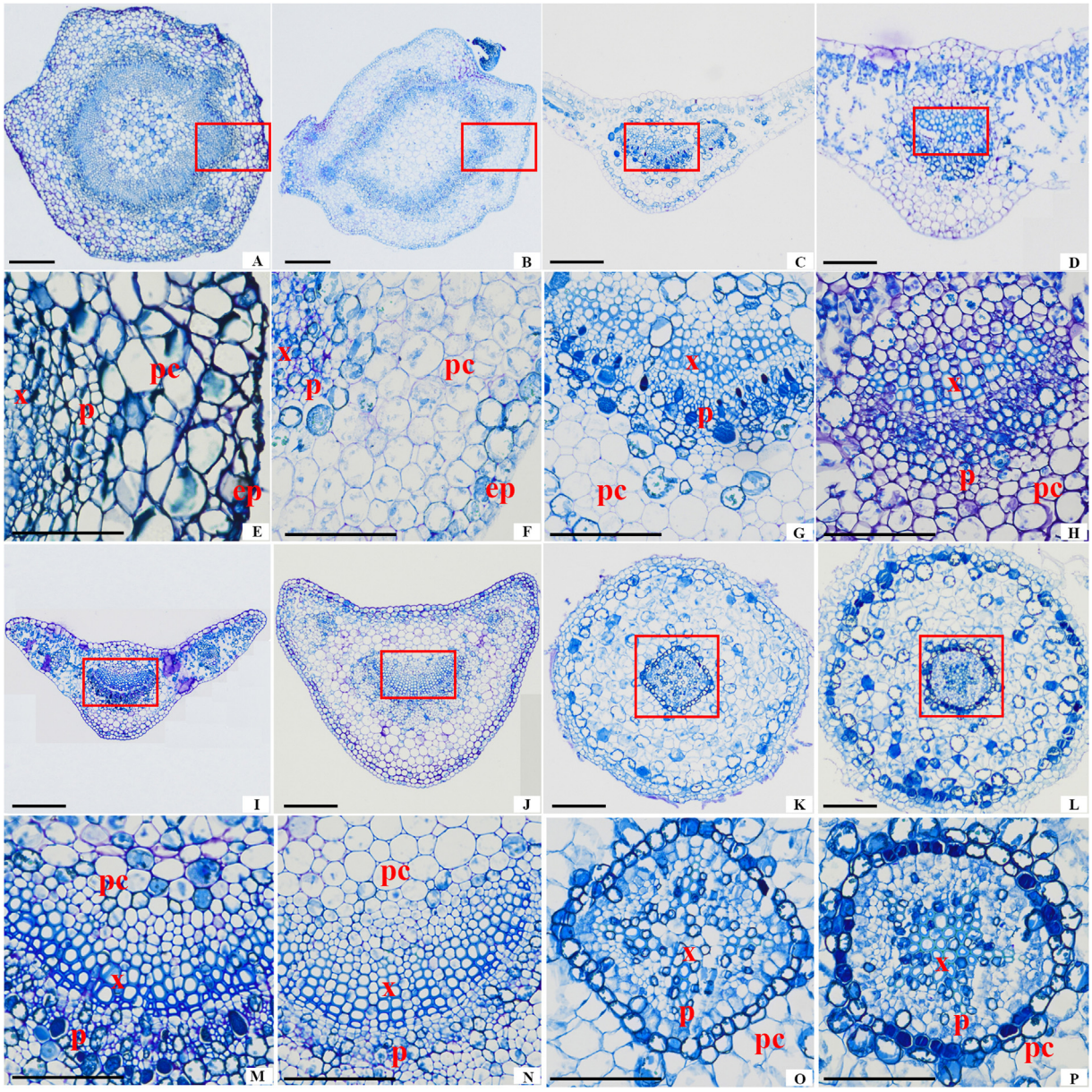


Fig. 4 Anatomical analysis of different tissues of the *in vitro*-grown 'PY-9' and 'Zhengdu' plantlets

(A and B) Transverse section of the stem of 'PY-9' and 'Zhengdu', respectively. (C and D) Transverse section of the leaf of 'PY-9' and 'Zhengdu', respectively. (E–H) Magnified views of the red-boxed areas in A–D, respectively. (I and J) Transverse section of the petiole of 'PY-9' and 'Zhengdu', respectively. (K and L) Transverse section of the root of 'PY-9' and 'Zhengdu', respectively. (M–P) Magnified views of the red-boxed areas in I–L, respectively. x, xylem; p, phloem; pc, parenchyma cells; ep, epidermis. Scale bars = 1 mm.

resulting in a significant difference of the chlorophyll T content between 'PY-9' and 'Zhengdu'. 'PY-9' also showed a much higher net photosynthetic rate, stomatal conductance, and transpiration rate than those of 'Zhengdu', whereas the intercellular CO_2 concentration of 'PY-9' and 'Zhengdu' was at the same level (Fig. 3).

3.3. *Anatomical comparison*

For the *in vitro*-grown plants, the 'PY-9' stem contained more well-developed vascular bundles with denser and greater numbers of cells in the xylem and phloem areas than those of the 'Zhengdu' stem (Fig. 4, A, B, E, F). In the leaves, the number of parenchyma cells of 'Zhengdu' was higher than that of 'PY-9', whereas the cell size of 'Zhengdu' was smaller in the parenchyma and phloem tissue (Fig. 4, C, D, G, H). In the leaf petiole, the cells of the xylem of 'Zhengdu' showed a more regular arrangement than those of 'PY-9'. By contrast, 'PY-9' had a greater size and number of cells in the phloem area than those of 'Zhengdu' (Fig. 4, I, J, M, N). In the root, 'PY-9' and 'Zhengdu' had a similar size and number of cells in the xylem, phloem, and parenchyma areas (Fig. 4, K, L, O, P).

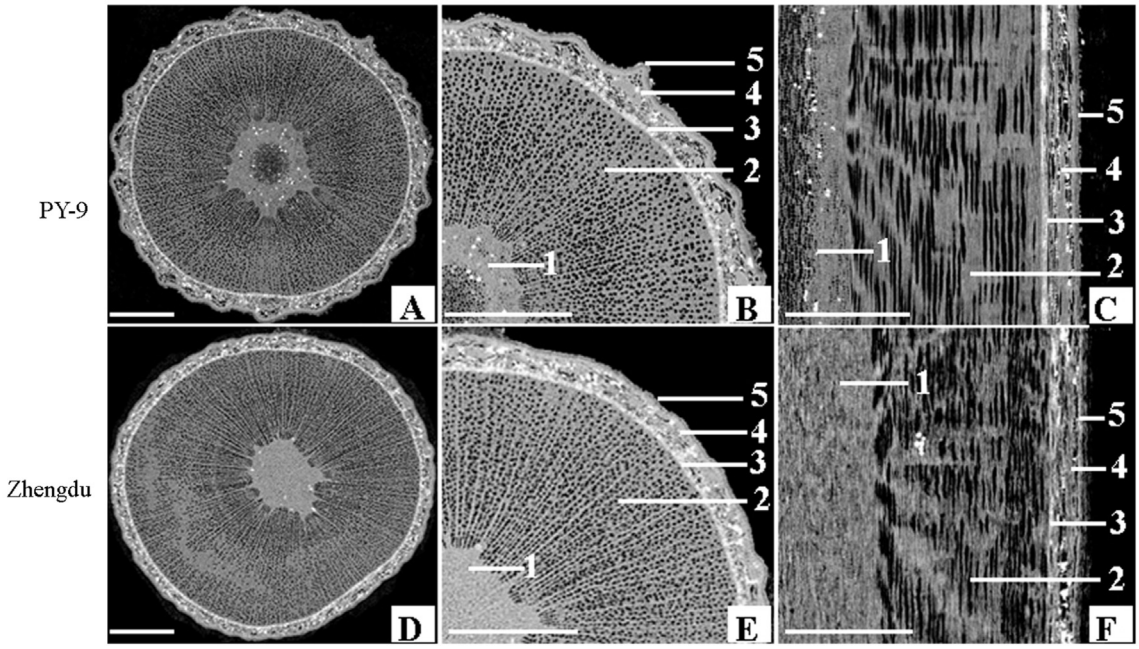


Fig. 5 Representative transverse (A, B, D, E) and longitudinal (C, F) X-ray computed tomography images
1. Pith tissue; 2, Xylem tissues; 3, Phloem tissues; 4, Cortex tissues; 5, Epidermis. Scale bars = 2 mm.

3.4. *Structural properties*

To obtain more details of the structural properties of the two rootstocks, X-ray computed tomography scanning, a non-destructive method, was applied to analyze the 2D and 3D structural properties of the field-grown shoot of 'PY-9' and 'Zhengdu'. From both the transverse and longitudinal 2D projections, different tissues of the pith, xylem, phloem, cortex, and epidermis could be recognized (Fig. 5). Compared to that of 'Zhengdu', the pith area of 'PY-9' showed a more porous structure (Fig. 5, A, D). A greater proportion of the bark (the area from the phloem to the epidermis) of 'PY-9' was also observed than that of 'Zhengdu' (Fig. 5, B, C, E, F). Much thinner and longer pores on the longitudinal slice were found in 'Zhengdu' compared to 'PY-9' (Fig. 5, C, F). Smaller sizes but greater numbers of pores on the transverse slice were found in 'Zhengdu' compared to 'PY-9'

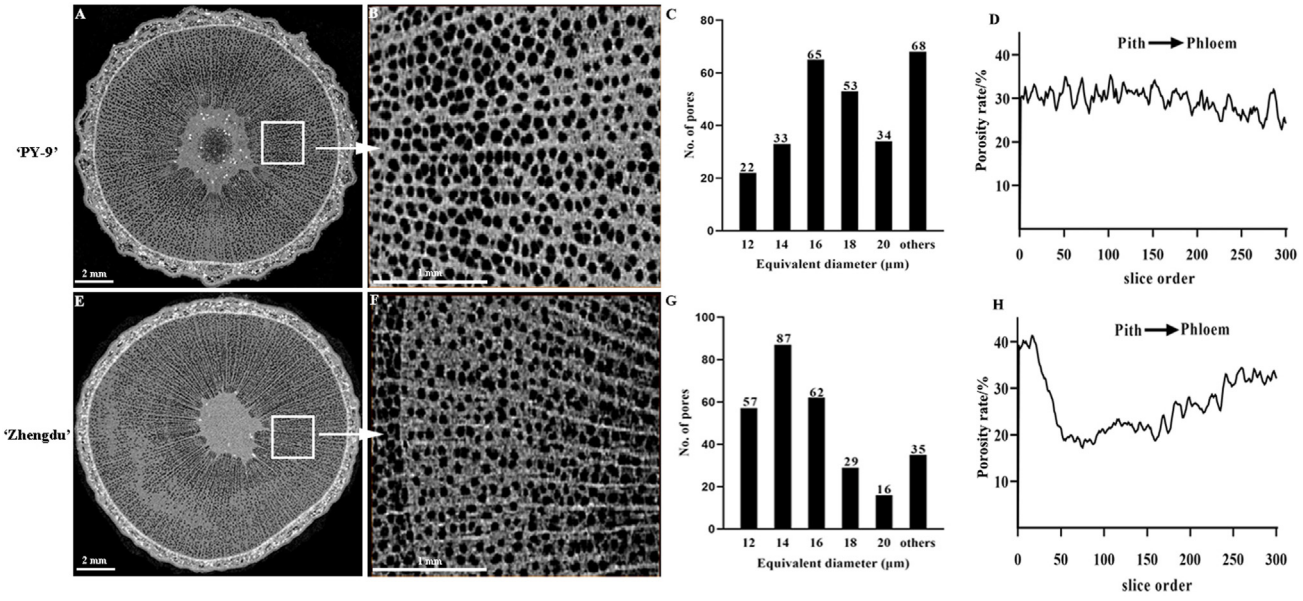


Fig. 6 Microstructural analysis of the transverse plane of the stem
(A and E) Transverse images of 'PY-9' and 'Zhengdu,' respectively. (B and F) Magnified views of the areas marked by rectangles in A and E, respectively. (C and D) Pore structure analysis of (B). (G and H) Pore structure analysis of (F).

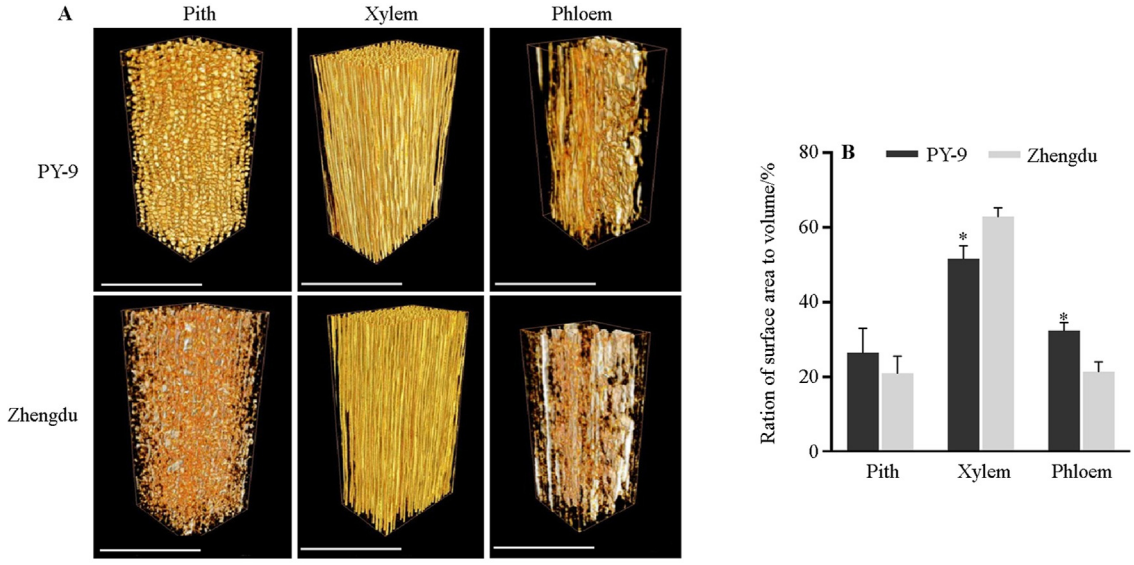


Fig. 7 Structural analysis of the pith, xylem, and phloem tissues

(A) Three-dimensional renderings reconstructed from a 100 μm × 100 μm × 300 μm volume of each tissue. (B) Analysis of the surface area of the tissues shown in panel (A). Scale bars in (A) = 100 μm. Bars in (B) represent mean ± *SD* of three replicate experiments. * means significant differences at $P < 0.05$.

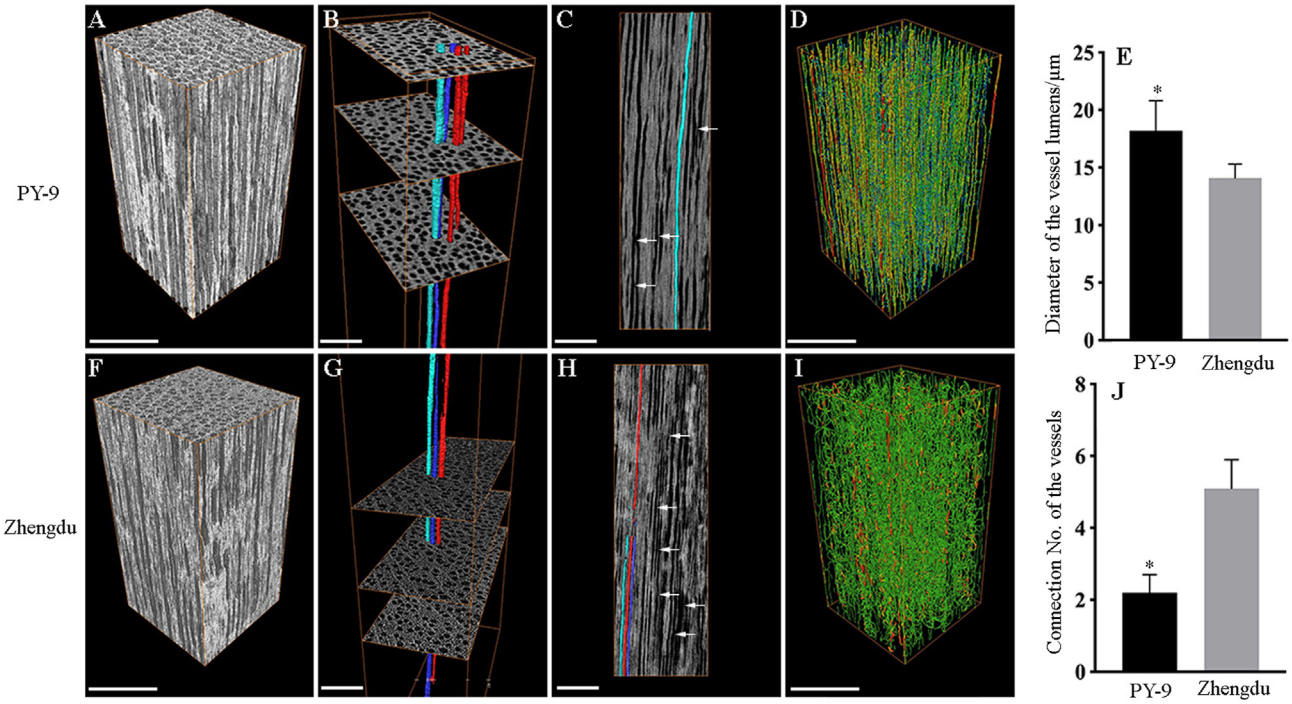


Fig. 8 Structural and spatial arrangement of xylem vessels from a 100 μm × 100 μm × 300 μm volume of the shoot stem assessed by X-ray scanning

(A and F) Three-dimensional (3D)-reconstructed model of 'PY-9' and 'Zhengdu', respectively. (B and G) Representative isolated 3D-reconstructed vessels with three transverse planes of 'PY-9' and 'Zhengdu', respectively; the color lines indicate the isolated 3D reconstructed vessels and the black areas on the plane indicate the transverse section of the vessels. (C and H) Two-dimensional longitudinal section of xylem vessels of 'PY-9' and 'Zhengdu', respectively; black areas indicate the vessels, dark gray areas indicate the xylem tissues, color lines indicate the marked vessel lumens, and white arrows indicate the intervessel connections. (D and I) The 3D-reconstructed skeleton of the xylem tissues of 'PY-9' and 'Zhengdu', respectively. (E and J) Structural property analysis of the vessels. Scale bars = 50 μm. Bars in (E) and (J) represent mean ± *SD* of three replicate experiments. * means significant differences at $P < 0.05$.

(Fig. 6, A, B, E, F), which was consistent with the observation on the longitudinal slice (Fig. 4, C, F). In the xylem area of 'PY-9', the most frequent size of the equivalent diameter of the pore was 16 μm, followed by 18 μm, 20 μm, 14 μm, and 12 μm (Fig. 6, C). However, in the xylem area of 'Zhengdu', the most frequent size of the equivalent diameter of the pore was 14 μm, followed by 16 μm, 12 μm, 18 μm, and 20 μm (Fig. 6, G). The xylem of 'PY-9' showed a stable porosity from the pith to the phloem with an average of 29.8% (Fig. 6, D). However, the porosity of the xylem tissue of 'Zhengdu' was the highest at ~40% and dropped down to ~20%, followed by an increase up to ~35%, with an average of 28.5% from the pith area to the phloem area (Fig. 6, H). No significant difference in xylem porosity was found between 'PY-9' and 'Zhengdu'.

Fig. 7, A shows representative 3D images with renderings of the pith, xylem, and phloem tissues from a 100 μm × 100 μm × 300 μm volume. Among the three tissues, the xylem displayed a more regular and compact shape, followed by the pith, while the phloem presented an irregular shape in both 'PY-9' and 'Zhengdu'. Compared to that of 'Zhengdu', the pith of 'PY-9' showed a more regular shape with obvious pores distributed inside the tissues (Fig. 7, A). No significant difference in the ratio of surface area to volume of the pith was found between 'PY-9' and 'Zhengdu'. However, in the xylem tissue, the ratio of surface area to volume of 'Zhengdu' was higher than that of 'PY-9'. By contrast, the ratio of surface area to volume of 'PY-9' was significantly higher than that of 'Zhengdu' in the phloem (Fig. 7, B).

To focus on the xylem structural properties, a 3D model of the vessels was reconstructed for both 'PY-9' and 'Zhengdu' (Fig. 8, A, F). Analysis of the isolated vessels and transverse planes from the tissues demonstrated a greater diameter and smaller number of vessels in the 'PY-9' xylem than in the 'Zhengdu' xylem (Fig. 8, B, G). Analysis of the longitudinal slice of the xylem showed a wider diameter and smaller number of vessels in 'PY-9' compared to 'Zhengdu' (Fig. 8, C, H), which was consistent with the transverse observation (Fig. 8, B, G). The 3D-reconstructed skeleton of the vessels also exhibited a different level of network connectivity between 'PY-9' and 'Zhengdu' (Fig. 8, D, I). These 2D and 3D observations on the appearances and network connectivity of the vessels were also supported by the statistical analysis showing that vessels in the xylem of 'PY-9' had a significantly greater diameter and lower level of intervessel connections than those of 'Zhengdu' (Fig. 8, E, J).

4. Discussion

The lack of suitable rootstocks that can effectively control scion growth has limited the development of intensive orchards in pear production (Cui et al., 2021), which has been partly attributed to poor understanding of the dwarfing mechanism (Knäbel et al., 2015). Rootstock-induced dwarfing is a difficult-to-measure trait that can be influenced by many factors, including tree age, soil type, climate, and the interaction between the rootstock and scion genotype (Harrison et al., 2016). Therefore, characterization of the morphology, growth, physiology, and tissue structure properties is essential for the development and application of an excellent dwarfing rootstock, which will in turn facilitate further exploration of the molecular mechanisms underlying rootstock-induced dwarfing (Tombesi et al., 2010; Hayat et al., 2021). In the present study, we analyzed the characteristics of a dwarfing *P. betulaefolia* 'PY-9' and a normal *P. betulaefolia* 'Zhengdu' under both *in vitro* and field-grown conditions. In addition to morphological and physiological characteristics, the details of the vascular structural properties were comprehensively investigated using both paraffin slicing and X-ray computed tomography scanning methods, which revealed the vessel structural variations in the dwarfing phenotype of *P. betulaefolia* and normal *P. betulaefolia* 'Zhengdu'.

More than 10 years after being transplanted in the germplasm nursery, the tree height of 'PY-9' was only half that of 'Zhengdu'. The shoot of 'PY-9' was much shorter with a more compact internodes and greater diameter compared with those of 'Zhengdu', which was consistent with the morphological characteristics of another dwarfing pear cultivar (*Pyrus communis*) reported by Liu et al. (2022). A shorter internode was also observed in a dwarfing hybrid (*P. betulaefolia*), which primarily induced the dwarfing phenotype (Tang et al., 2022). This suggested that 'PY-9' is a stable dwarfing-type mutant of *P. betulaefolia*, with potential ability to control the scion growth size when used as a rootstock. Notable differences in the shoot growth rate between 'PY-9' and 'Zhengdu' were detected from 20 days to 40 days after full bloom, indicating that the physiological and metabolic differences during this period affected the final shoot length in the growing season. In apple, the shoot growth rate was reported to reach the peak at approximately 40 days after bud break, although significant differences in the growth rate and length of shoot were not observed until 112 days after bud break between a dwarfing ('Fuji'/'M9') and non-dwarfing ('Fuji'/'MM106') grafted tree (Song et al., 2016). The time difference in the phenological phases between apple and pear could explain the different results between studies. The greatest water potential tension of 'PY-9' and 'Zhengdu' was detected at 30 days after full bloom in our study, which was likely due to the active metabolism activities (e.g. transpiration and respiration), coinciding with the fast-growing period of the shoots.

We found higher photosynthetic efficiency in 'PY-9' than in 'Zhengdu', which could be explained by the greater leaf chlorophyll content, leaf area and leaf thickness of 'PY-9' compared to those of 'Zhengdu'. Similar findings were also reported by Liu et al. (2022), in which the dwarf pear variety '601D' had stronger photosynthetic capacity than the non-dwarf pear '601T'. However, it has also been reported that in some cases dwarfing might be caused by lower stomatal conductance and photosynthetic rate (Hayat et al., 2021), which is opposite to the observation in our study. Therefore, it is hard to correlate photosynthetic activity with tree dwarfing so far. Although no significant difference in plant height was found between the *in vitro*-grown 'PY-9' and 'Zhengdu' plantlets, 'Zhengdu' had more branches than 'PY-9'. This indicated a higher level of endogenous hormones and/or higher sensitivity to exogenous hormones in 'Zhengdu' plantlets. However, this hypothesis needs further validation. In previous studies investigating the dwarfing mechanism, the alteration of plant hormones was proposed to contribute to the differences observed in shoot length and tree size in several crops, including

apple (Li et al., 2012; Zhang et al., 2015; Song et al., 2016; Tworkoski and Fazio, 2016), pear (Liu et al., 2022; Zheng et al., 2022), peach (Sorce et al., 2002), and litchi (Hu et al., 2018).

Anatomical characteristics have long been linked to the dwarfing traits of fruit trees, which was also a focus point of our research. In an anatomical comparison of dwarf-type and normal-type pears, smaller vessel diameter and vessel density were found in the former, and the dwarf-type pear also exhibited thicker leaves and more cell layers in the palisades (Chen et al., 2015). A shorter cell length or fewer cortical parenchyma cells was considered to induce the shorter internode of the dwarfing type in pear (Chen et al., 2015), apple (Ma et al., 2016; Yan et al., 2022), and wheat (Wang et al., 2016). By contrast, the size of the cortical parenchyma cells of the dwarf-type pear was reported to be larger than that of the non-dwarf pear (Tang et al., 2022). Our anatomical observation showed that 'PY-9' had a greater number of cells in the vascular tissues than 'Zhengdu', 'Zhengdu' had a greater number and smaller size of cells in the parenchyma of the leaf than 'PY-9', and 'PY-9' had a greater size and number of cells with irregular arrangement in the vascular tissues of the petiole than 'Zhengdu'. These differences indicated that the dwarfing induced by physiological mechanisms varies among tissues and species.

Even though no direct experimental evidence was provided to show the dwarfing capability of 'PY-9', we investigated the important traits, which are relevant to dwarfing capacity of rootstocks. Those traits including lower weight, higher percentage of stem cortical tissue, thicker leaves and lower water potential tension of the growing season, which are accordant with the traits in the previously identified apple rootstocks with obvious dwarfing capacity (Dejong et al., 2013; Harrison et al., 2016; Feng et al., 2018, 2022). All these data and comparisons suggested that the dwarf-type pear 'PY-9' is a potential rootstock with dwarfing capacity.

X-ray scanning observations showed that field-grown 'PY-9' had a greater proportion of the bark (from phloem to epidermis) than that of 'Zhengdu', which was supported by the anatomical analysis results of *in vitro*-grown 'PY-9' and 'Zhengdu' plantlets. Consistently, a greater proportion of the bark in root was also observed in a dwarfing apple rootstock, which was considered to be associated with the rootstock-induced dwarfing capacity (Harrison et al., 2016). Therefore, a higher proportion of the bark is possibly associated with the ability of the rootstock to reduce scion growth. Based on the 2D and 3D reconstruction analysis, we found that 'PY-9' had a wider diameter and fewer number of the vessels than those of 'Zhengdu', whereas 'ZhengduD' had a higher level of intervessel connectivity than 'PY-9'. Higher intervessel connectivity of the vessels likely results in high hydraulic conductance, which can explain why 'Zhengdu' had higher water potential tension than 'PY-9'. However, a smaller vessel diameter was associated with the dwarfing phenotype in previous studies, including pear (Chen et al., 2015), peach (Tombesi et al., 2010), citrus (Saeed et al., 2010), and cherry (Zorić et al., 2012). Those studies also found that a smaller vessel diameter could increase the water resistance and result in lower tree vigor, which was opposite to our findings. Therefore, our finding that the lower intervessel connectivity in the dwarfing phenotype 'PY-9' decreased the water potential tension in the plant and resulted in fewer tree growth than that of 'Zhengdu' in the growing season provides new insights into the physiological mechanisms involved in the dwarfism of pear.

Plant vessel embolisms reduce hydraulic conductance (Knipfer et al., 2015b), and embolism removal is critical for restoring hydraulic pathways in some plants (Brodersen et al., 2017). Embolism susceptibility is associated with xylem network characteristics, which influence the water and nutrient transport efficiency, especially in an environment of drought stress (Knipfer et al., 2018). Our previous study proved that intervessel connectivity and the ratio of the surface area to the volume of the xylem elements influenced the hydraulic conductance in the peduncle of the pear fruit (Cui et al., 2022). Therefore, we speculate that the higher intervessel connectivity and ratio of surface area to volume of the xylem tissues in 'Zhengdu' help to overcome the influence of embolism and increase the hydraulic conductance, which contribute to the vigorous growth of the tree.

5. Conclusions

The physiological mechanisms involved in the dwarfing of fruit trees have been intensively investigated. Our results showed that 'PY-9' is a stable dwarfing type of *P. betulaefolia* with potential application to control scion growth in pear production. The dwarfing mechanism of 'PY-9' suggested from this study is different from that proposed in other studies of pear and apple, indicating interspecific variations of the dwarfing mechanism in plants. With the help of X-ray computed tomography analysis in a 3D view, this study provides the first evidence that intervessel connectivity of the xylem is associated with dwarfing in pear trees.

Declaration of interests

The authors declare that they have no known competing financial interests or personal relationships that could have appeared to influence the work reported in this paper.

Acknowledgments

This work was supported by grants from the Agriculture Science and Technology of Shandong Province (Grant No. 2019YQ015), the Agricultural Variety Improvement Project of Shandong Province (Grant No. 2022LZGC011), and the earmarked fund for CARS (Grant No. CARS-28-07).

REFERENCES

Brodersen, C.R., Thorsten, K., Mcelrone, A.J., 2017. *In vivo* visualization of the final stages of xylem vessel refilling in grapevine (*Vitis vinifera*) stems. New Phytol, 217: 117–126.

Chen, B., Wang, C., Tian, Y., Chu, Q., Hu, C., 2015. Anatomical characteristics of young stems and mature leaves of dwarf pear. Sci Hortic, 186: 172–179.

Cui, Z.H., Aguero, C.B., Wang, Q.C., Walker, M.A., 2019. Validation of micrografting to identify incompatible interactions of rootstocks with virus-infected scions of Cabernet Franc. Aust J Grape Wine Res, 25: 268–275.

Cui, Z., Zhang, H., Galarneau, E., Yang, Y., Li, D., Song, J., Ma, C., Zhang, S., Wang, R., 2021. Metabolome analysis reveals important compounds related to dwarfing effect of interstock on scion in pear. Ann Appl Biol, 179: 108–122.

Cui, Z., Sun, H., Lu, Y.Q., Ren, L.X., Xu, X.R., Li, D.L., Wang, R., Ma, C.H., 2022. Variations in pedicel structural properties among four pear species (*Pyrus*): insights into the relationship between the fruit characteristics and the pedicel structure. Front Plant Sci, 13: 815283.

Dejong, T.M., Tombesi, S., Basile, B., Silva, D., 2013. Beakbane and Thompson (1939,East Malling) had it right: scion vigour is physiologically linked to the xylem anatomy of the rootstock. Aspect Appl Biol, 17: 51–58.

Fazio, G., Wan, Y., Kviklys, D., Romero, L., Adams, R., Strickland, D., Robinson, T., 2014. *Dw2*, a new dwarfing locus in apple rootstocks and its relationship to induction of early bearing in apple scions. J Am Soc Hortic Sci, 139: 87–98.

Feldkamp, L.A., Davis, L.C., Kress, J.W., 1984. Practical cone-beam algorithm. J Opt Soc Am, 1: 612–619.

Feng, C., Huang, X.W., Li, X.L., Zhou, J., Li, T.H., 2022. Comparative study on drought resistance of different apple dwarfing rootstock and scion combinations. Acta Hortic Sin, 49: 945–957. (in Chinese)

Feng, Y., Xu, X.F., Zhang, X.Z., Wu, T., Wang, Y., Han, Z.H., 2018. Progress of dwarfing mechanism of apple rootstock. Acta Hortic Sin, 45: 1633–1641. (in Chinese)

Foster, T., Celton, J., Chagné, D., Tustin, D., Gardiner, S., 2015. Two quantitative trait loci, *Dw1* and *Dw2*, are primarily responsible for rootstock-induced dwarfing in apple. Hortic Res, 2: 15001.

Harrison, N., Harrison, R., Nuria, B., Lopez, E., Medina, M., Lipska, M., Ruíz, R., Brain, P., Gregory, P., Fernández, F., 2016. A new three-locus model for rootstock-induced dwarfing in apple revealed by genetic mapping of root bark percentage. J Exp Bot, 67: 1871–1881.

Hayat, F., Iqbal, S., Coulibaly, D., Razzaq, M., Nawaz, M., Jiang, W., Shi, T., Gao, H., 2021. An insight into dwarfing mechanism: contribution of scion-rootstock interactions toward fruit crop improvement. Fruit Res, 1: 3.

Hu, F., Chen, Z., Zhao, J., Wang, X., Su, W., Qin, Y., Liu, J.H., 2018. Differential gene expression between the vigorous and dwarf litchi cultivars based on RNA-seq transcriptome analysis. PLoS One, 13: 12.

Knäbel, M., Friend, A., Palmer, J., Diack, R., Wiedow, C., Alspach, P., Deng, C., Gardiner, S., Tustin, D., Schaffer, R., Foster, T., Chagné, D., 2015. Genetic control of pear rootstock-induced dwarfing and precocity is linked to a chromosomal region syntenic to the apple *Dw1* loci. BMC Plant Biol, 15: 230.

Knipfer, T., Eustis, A., Brodersen, C., Walker, A.M., Mcelrone, A.J., 2015a. Grapevine species from varied native habitats exhibit differences in embolism formation/repair associated with leaf gas exchange and root pressure. Plant Cell Environ, 38: 1503–1513.

Knipfer, T., Fei, J., Gambetta, G.A., Mcelrone, A.J., Matthews, M.A., 2015b. Water transport properties of the grape pedicel during fruit development: insights into xylem anatomy and function using microtomography. Plant Physiol, 168: 1590–1602.

Knipfer, T., Barrios-Masias, F.H., Cuneo, I.F., Bouda, M., Mcelrone, A.J., 2018. Variations in xylem embolism susceptibility under drought between intact saplings of three walnut species. Tree Physiol, 38: 1180–1192.

Li, L.H., Zhang, H., Yu, C., Ma, L., Wang, Y., Zhang, X.Z., Han, Z.H., 2012. Possible roles of auxin and zeatin for initiating the dwarfing effect of M9 used as apple rootstock or interstock. Acta Physiol Plant, 34: 235–244.

Li, J.W., Wang, B., Song, X.M., Wang, R.R., Chen, L., Zhang, Z.B., Wang, Q.C., et al., 2013. Potato leafroll virus (PLRV) and potato virus y (PVY) influence vegetative growth, physiological metabolism, and microtuber production of *in vitro*-grown shoots of potato (*Solanum tuberosum* L.). Plant Cell Tissue Organ Cult, 114: 313–324.

Li, W., Tian, Y.K., Wang, C.H., Bai, M.D., Hou, D.L., 2015. Screening of SNP markers tightly linked to PcDw locus determining pear dwarf trait using HRM technology. Acta Hortic Sin, 42: 214–220. (in Chinese)

Liu, J., Zhang, C., Li, T., Liang, C., Yang, Y., Li, D., Cui, Z., Wang, R., Song, J., 2022. Phenotype and mechanism analysis of plant dwarfing in pear regulated by abscisic acid. J Integr Agric, 21: 1346–1356.

Ma, Y., Xue, H., Zhang, L., Zhang, F., Ou, C., Wang, F., Zhang, Z., 2016. Involvement of auxin and brassinosteroid in dwarfism of autotetraploid apple (*Malus* × *domestica*). Sci Rep, 6: 26719.

Marín, D., Miranda, C., Abad, F.J., Urrestarazu, J., Mayor, B., Villa-Llop, A., Santesteban, L.G., 2023. Agronomic evaluation of eight 41 B × 110 richter grapevine genotypes as rootstock candidates for mediterranean viticulture. Hortic Plant J, 9: 720–728.

Olmstead, M., Lang, N., Ewers, F., Owens, S., 2006. Xylem vessel anatomy of sweet cherries grafted onto dwarfing and nondwarfing rootstocks. J Am Soc Hortic Sci, 131: 577–585.

Ou, C., Jiang, S., Wang, F., Tang, C., Hao, N., 2015. An RNA-seq analysis of the pear (*Pyrus communis* L.) transcriptome, with a focus on genes associated with dwarf. Plant Gene, 4: 69–77.

Petri, C., Alburquerque, N., Faize, M., Scorza, R., Dardick, C., 2018. Current achievements and future directions in genetic engineering of European plum (*Prunus domestica* L.). Transgenic Res, 27: 225–240.

Pilcher, R.L., Celton, J.M., Gardiner, S.E., 2008. Genetic markers linked to the dwarfing trait of apple rootstock 'Malling 9'. J Am Soc Hortic Sci, 133: 100–106.

Saeed, M., Dodd, P., Sohail, L., 2010. Anatomical studies of stems, roots and leaves of selected citrus rootstock varieties in relation to their vigour. J Hortic For, 2: 87–94.

Scholander, P.F., Hammel, H.T., Bradstreet, E.D., Hemmingsen, E.A., 1965. Sap pressure in vascular plants. Science, 148: 339–346.

Song, C., Zhang, D., Zhang, J., Zheng, L., Han, M., 2016. Expression analysis of key auxin synthesis, transport, and metabolism genes in different young dwarfing apple trees. Acta Physiol Plant, 38: 43.

Sorce, C., Massai, R., Picciarelli, P., Lorenzi, R., 2002. Hormonal relationships in xylem sap of grafted and ungrafted *Prunus* rootstocks. Sci Hortic, 93: 333–342.

Tang, Z.K., Sun, M.Y., Jia-Ming, L.I., Song, B.B., Liu, Y.Y., Tian, Y.K., Wang, C.H., Wu, J., 2022. Comparative transcriptome analysis provides insights into the mechanism of pear dwarfing. J Integr Agric, 21: 1952–1967.

Tombesi, S., Johnson, R., Day, K., DeJong, T.M., 2010. Interactions between rootstock, inter-stem and scion xylem vessel characteristics of peach trees growing on rootstocks with contrasting size-controlling characteristics. Ann Bot, 105: 327–331.

Tworkoski, T., Fazio, G., 2016. Hormone and growth interactions of scions and size-controlling rootstocks of young apple trees. Plant Growth Regul, 78: 105–119.

Venema, J., Dijk, B., Bax, J., Van-Hasselt, P., Elzenga, J.T.M., 2008. Grafting tomato (*Solanum lycopersicum*) onto the rootstock of a high-altitude accession of *Solanum habrochaites* improves suboptimal-temperature tolerance. Environ Exp Bot, 63: 359–367.

Weibel, A.M., 2008. Dwarfing Mechanisms of *Prunus* Species as Interstems and Rootstocks on Peach [*Prunus persica* (L.) Batsch] Tree Vegetative Growth and Physiology. [Ph. D. Dissertation]. Clemson: Clemson University.

Wang, Y., Xiao, X., Wang, X., Zeng, J., Kang, H., Fan, X., Sha, L., Zhang, H., Zhou, Y., 2016. RNA-Seq and iTRAQ reveal the dwarfing mechanism of dwarf polish wheat (*Triticum polonicum* L.). Int J Biol Sci, 12: 653–666.

Wu, J., Wang, Z., Shi, S., Zhang, R., Ming, S., Zhu, M., Khan, S., Tao, S., Korban, H., Wang, J., Chen, T., Nishio, X., Xu, L., Cong, K., Qi, X., Huang, Y., Wang, X., Zhao, J., Wu, C., Deng, C., Gou, W., Zhou, H., Yin, G., Qin, Y., Sha, Y., Tao, H., Chen, Y., Yang, Y., Song, D., Zhan, J., Wang, L., Li, M., Dai, C., Gu, Y., Wang, D., Shi, X., Wang, H., Zhang, L., Zeng, D., Zheng, C., Wang, M., Chen, G., Wang, L., Xie, V., Sovero, S., Sha, W.,

Huang, S., Zhang, M., Zhang, J., Sun, L., Xu, Y., Li, X., Liu, Q., Li, J., Shen, J., Wang, R., Paull, J., Bennetzen, J., Zhang, S., 2013. The genome of the pear (*Pyrus bretschneideri* Rehd.). Genome Res, 23: 396–408.

Yan, T., Mei, C., Song, H., Shan, D., Sun, Y., Hu, Z., Wang, L., Zhang, T., Wang, J., Kong, J., 2022. Potential roles of melatonin and ABA on apple dwarfing in semi-arid area of Xinjiang China. Peer J, 10: e13008.

Zhang, H., An, H.S., Wang, Y., Zhang, X.Z., Han, Z.H., 2015. Low expression of PIN gene family members is involved in triggering the dwarfing effect in M9 interstem but not in M9 rootstock apple trees. Acta Physiol Plant, 37: 104–121.

Zheng, X., Li, Y., Ma, C., Chen, B., Sun, Z., Tian, Y., Wang, C., 2022. A mutation in the promoter of the arabinogalactan protein 7-like gene *PcAGP7-1* affects cell morphogenesis and brassinolide content in pear (*Pyrus communis* L.) stems. Plant J, 109: 47–63.

Zorić, L., Ljubojević, M., Merkulov, L., Luković, J., Ognjanov, V., 2012. Anatomical characteristics of cherry rootstocks as possible preselecting tools for prediction of tree vigor. J Plant Growth Regul, 31: 320–331.